SUPPLEMENTARY MATERIAL

Comparison of the retinal structure of CaChR1 and CrChR2 from the fingerprint region along with photoreversibility of the two primary photointermediates.

A significantly different pattern is observed in the fingerprint region for the 80 K FTIR-difference spectrum of *Cr*ChR2 compared to *Ca*ChR1 (Figure 1). Although a negative band still appears at 1205 cm^{-1} and a positive shoulder at 1196 cm^{-1}, a more positive band appears at 1190 cm^{-1} and the negative band near 1165-1170 cm^{-1} is replaced by a negative band at 1179 cm^{-1}. These alterations are most likely explained by the presence of 13-*cis* retinal in both the dark and light-adapted state of *Cr*ChR2 (1) which also isomerizes during the primary phototransition and contributes to the difference spectrum in this region. Indeed, a similar conclusion was reached from the FTIR-difference spectrum for the primary phototransition of blue absorption proteorhodopsin (BPR) (2), where a second positive band appears at 1188 cm^{-1} and the band between 1165-1170 cm^{-1} is absent. Supporting this conclusion, a positive band appears in the RRS of *Cr*ChR2 (1,3) at 1185 cm^{-1} which most likely accounts for the negative band at 1179 cm^{-1} in the FTIR-difference spectrum, which is downshifted due to spectral splitting with the positive band at 1190 cm^{-1}. Note that while these differences might be attributed to the fact that *Cr*ChR2 was reconstituted in DMPC and *Ca*ChR1 in ECPL (see Materials and Methods), identical results were obtained for *Cr*ChR2 reconstituted in ECPL (Figure S1).

Evidence for isomerization of a pure all-*trans* retinal in the primary phototransition of *Ca*ChR1 and mixed all-*trans*/13-*cis* isomerization in *Cr*ChR2 can be found from photoreversibility experiments. The *Cr*ChR2 difference spectrum shown in Figure 1 is the average of many cycles

of differences involving photo-excitation/reversal using 455 nm and 530 nm illumination light as described in Materials and Methods. In contrast, the difference spectrum recorded for only the initial push from the dark-adapted state to P1 (using only 455 nm illumination), differs somewhat in the fingerprint region, with a negative band appearing near 1184 cm^{-1} instead of 1179 cm^{-1} (see Figure S2). An almost identical difference spectrum involving only the first push was also reported earlier for *Cr*ChR2 at 80 K (4) despite the fact that it was in a detergent micellar form. This indicates that the first push at low temperature involves isomerization of even more 13-*cis* retinal since the 1183 cm^{-1} band is highly characteristic of this isomer (5,6). Consequently, the photoproduct of the 13-*cis* photocycle is not fully photo-reversed and thus the average of many photocycles does not match the first push. In contrast, the first push and the average of many photocycles of *Ca*ChR1 are nearly identical (see Figure S2), a consequence of the pure all-*trans* retinal content of both the dark and light-adapted *Ca*ChR1.

Assignment of Bands in the 1700-1800 cm^{-1} Region to Carboxylic Acid C=O Stretching Vibrations

A number of positive and negative bands appear in the 1700-1800 cm^{-1} region in the *Ca*ChR1→P1 difference spectrum (Figure 7A). Importantly, there is a significant different compared to *Cr*ChR2, where two prominent positive/negative bands appear at 1741/1736 cm^{-1} but most of the bands appearing in *Ca*ChR1 are absent (see Figure 1 and Figure S4).

Bands appearing in this region often reflect hydrogen bonding and protonation changes of individual Asp and Glu residues due to alterations in the C=O stretch frequency of the carboxylic acid groups (7). Note however, bands near and below 1700 cm^{-1} can also arise from the carboxyl

stretch mode of Asn and Gln residues (2,8). In the case of BR→K difference spectrum, a pair of weak negative/positive bands appears near 1741/1733 cm^{-1} (Figure 1) which were assigned on the basis of site-directed mutagenesis to Asp115 (9) located near the retinal β-ionone ring (10). Notably, no other bands in this region appear and thus it is unlikely that other Asp/Glu residues undergoing any significant alteration during the primary phototransition of the BR photocycle (9).

Assignment of bands in this region to Asp and Glu residues can be made by measuring the frequency downshift of the carboxylic acid C=O stretch mode that occurs upon H-D exchange (COOH→COOD). Depending on the strength of the hydrogen bonding, this exchange normally causes a downshift of the $\upsilon_{C=O}$ from 1-12 cm^{-1} with smaller shifts occurring for stronger hydrogen bonding (11). As shown in Figure 7 traces A (*Ca*ChR1 in H_2O) and F (*Ca*ChR1 in D_2O), all of the bands observed in this region downshift from 5-11 cm^{-1}. Note however that at least part of the apparent downshift of the positive band at 1703 cm^{-1} may be due to the overlap of hidden bands near 1708/1703 cm^{-1} which have downshifted due to H-D exchange from 1716/1710 cm^{-1} as indicated in *Ca*ChR1 mutants (see below). A smaller or even absent H-D induced shift of this band could be caused by very strong hydrogen bonding (for example see case of D96 in L intermediate of BR (11)), absence of H-D exchange which could also occur due to very strong hydrogen bonding, or if this vibration arose from an Asn or Gln residue. Note also that the negative band at 1687 cm^{-1} is unaffected by retinal changes or D/H exchange and most likely because of the lower frequency originates from an amide I mode of a buried peptide structure (e.g. inaccessible to H-D exchange) in the protein.

The non-chromophore origin of these bands (and high degree of reproducibility) can also be seen by comparison of this region with *Ca*ChR1 regenerated with the various retinals (Figure 7, spectra C-E). For example, the two retinal isotope substitutions have no effect on these bands. This insensitivity is especially notable for the case of the A2 retinal substitution (Figure 7, spectrum C) where the two hydrogens at the 3,4 position are eliminated in the β-ionone ring.

The effects of mutants in the carboxylic acid stretching region detected using FTIR double difference spectra (DDS)

The effects of the mutations can also be observed in the double difference spectrum (DDS) produced by interactively subtracting the mutant FTIR difference from the WT difference with a scaling factor that cancels bands at 1765 and 1760 cm^{-1}. For example, the DDS of D299E (Figure S6) displays a positive band at 1703 cm^{-1} and broad negative band near 1690 cm^{-1} which resolves into two separate negative components at 1691 and 1682 cm^{-1}. The pair of negative bands arises from the downshift of the 1703 cm^{-1} to 1696 cm^{-1} while the second component most likely arises from a drop in intensity of the negative 1688 cm^{-1} band tentatively assigned to an amide I mode. In the case of D299N and E169Q, the DDS spectra are almost identical, again illustrating the equivalent effects of these mutations in this region. Both display a positive band at 1703 cm^{-1} indicating the disappearance of this band assigned to D299. However, note that in this case the higher frequency component of the negative band near 1690 cm^{-1} does not appear, indicating there is no frequency downshift as in the case of D299E. In addition, a negative band appears at 1720 cm^{-1} corresponding to the negative band deduced to be present in WT and assigned to the deprotonation of Asp169. All of the mutants also appear to cause the

disappearance of the negative positive band at 1710/1716 cm^{-1} which is unassigned to any Asp/Glu group.

REFERENCES

1. Nack, M., Radu, I., Bamann, C., Bamberg, E., and Heberle, J. (2009) The retinal structure of channelrhodopsin-2 assessed by resonance Raman spectroscopy. *FEBS Lett 583*, 3676-3680
2. Amsden, J. J., Kralj, J. M., Bergo, V. B., Spudich, E. N., Spudich, J. L., and Rothschild, K. J. (2008) Different structural changes occur in blue- and green-proteorhodopsins during the primary photoreaction. *Biochemistry 47*, 11490-11498
3. Ogren, J. I., Mamaev, S., Russano, D., Li, H., Spudich, J. L., and Rothschild, K. J. (2014) Retinal chromophore structure and Schiff base interactions in red-shifted channelrhodopsin-1 from Chlamydomonas augustae. *Biochemistry 53*, 3961-3970
4. Radu, I., Bamann, C., Nack, M., Nagel, G., Bamberg, E., and Heberle, J. (2009) Conformational changes of channelrhodopsin-2. *J Am Chem Soc 131*, 7313-7319
5. Smith, S. O., Braiman, M. S., Myers, A. B., Pardoen, J. A., Courtin, J. M. L., Winkel, C., Lugtenburg, J., and Mathies, R. A. (1987) Vibrational analysis of the all-trans-retinal chromophore in light-adapted bacteriorhodopsin. *J. Am. Chem. Soc. 109*, 3108-3125
6. Smith, S. O., Pardoen, J. A., Lugtenburg, J., and Mathies, R. A. (1987) Vibrational analysis of the 13-cis-retinal chromophore in dark-adapted bacteriorhodopsin. *J. Phys. Chem. 91*, 804-819

7. Rothschild, K. J., Zagaeski, M., and Cantore, W. A. (1981) Conformational changes of bacteriorhodopsin detected by Fourier transform infrared difference spectroscopy. *Biochem Biophys Res Commun 103*, 483-489

8. Barth, A. (2000) The infrared absorption of amino acid side chains. *Progress in biophysics and molecular biology 74*, 141-173

9. Braiman, M. S., Mogi, T., Marti, T., Stern, L. J., Khorana, H. G., and Rothschild, K. J. (1988) Vibrational spectroscopy of bacteriorhodopsin mutants: light-driven proton transport involves protonation changes of aspartic acid residues 85, 96, and 212. *Biochemistry 27*, 8516-8520

10. Luecke, H., Schobert, B., Richter, H. T., Cartailler, J. P., and Lanyi, J. K. (1999) Structure of bacteriorhodopsin at 1.55 A resolution. *J Mol Biol 291*, 899-911

11. Maeda, A., Sasaki, J., Shichida, Y., Yoshizawa, T., Chang, M., Ni, B., Needleman, R., and Lanyi, J. K. (1992) Structures of aspartic acid-96 in the L and N intermediates of bacteriorhodopsin: analysis by Fourier transform infrared spectroscopy. *Biochemistry 31*, 4684-4690

Supplementary Figures

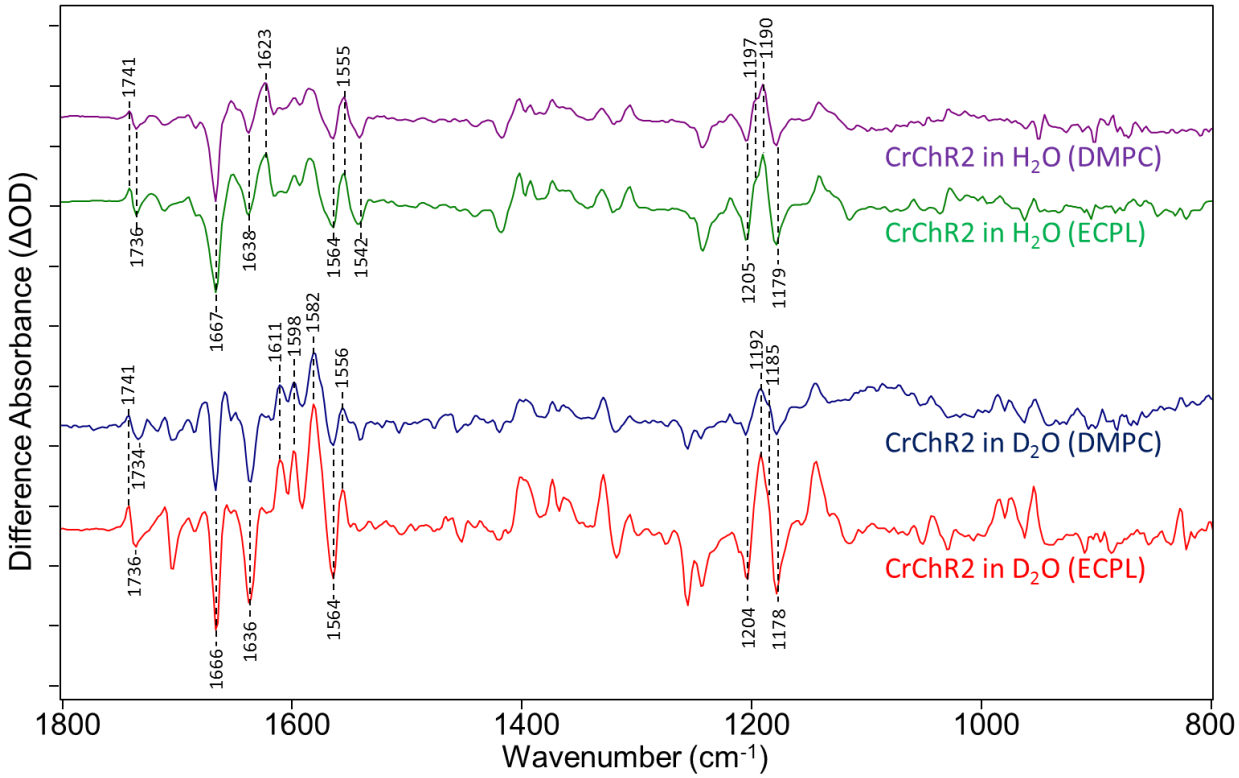

Figure S1: Comparison of *Cr*ChR2 reconstituted in DMPC (purple and blue traces) and ECPL (green and red traces) in both H_2O (top two traces) and D_2O (bottom two traces) over the 800-1800 cm^{-1} region at 80 K. Y-axis markers are approximately 0.5 mOD for the H_2O data and 0.2 mOD for the D_2O data.

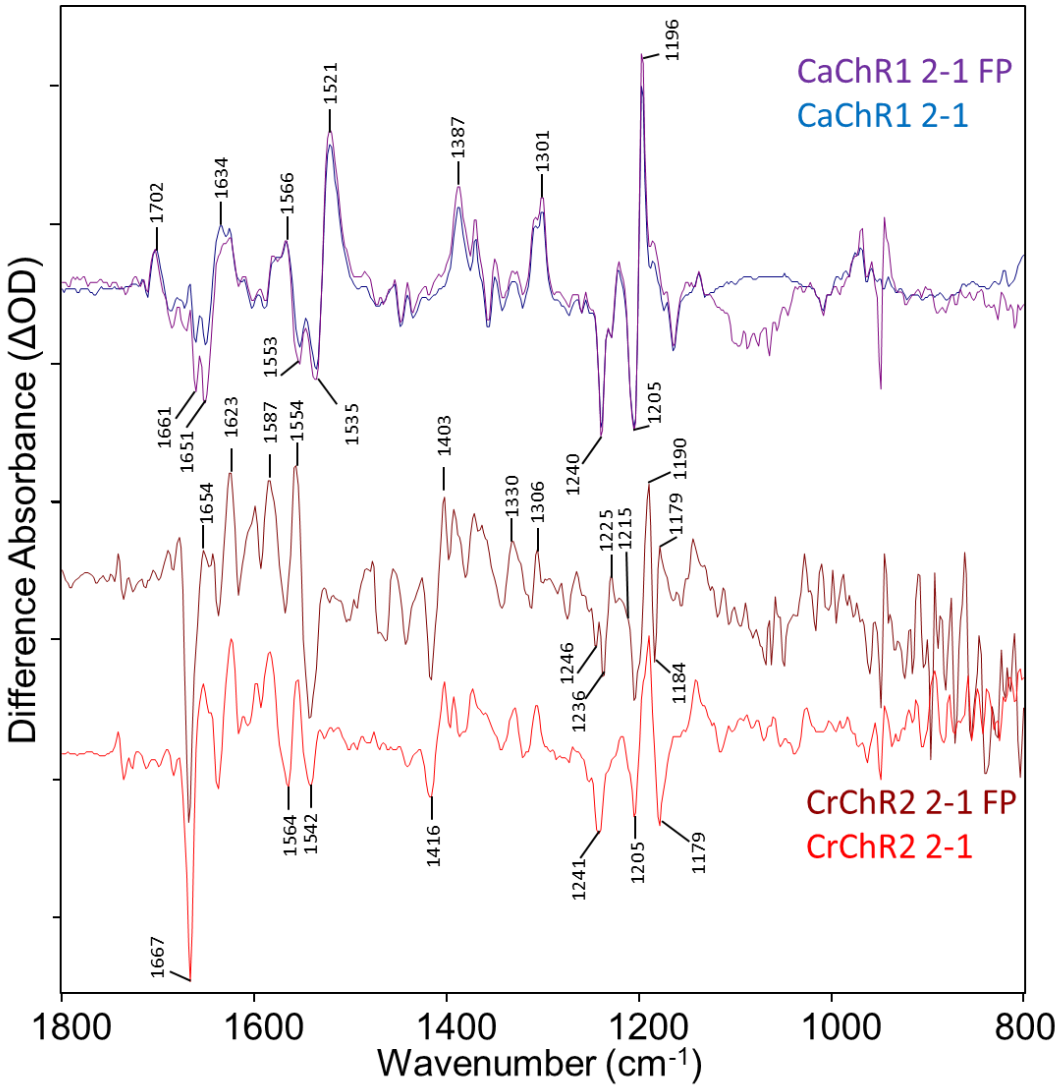

Figure S2: Comparison of *Ca*ChR1 and *Cr*ChR2 over the 800-1800 cm^{-1} region both for the "first push" (purple and maroon traces, respectively) and for many averages of photoexcitation/photoreversal (teal and red traces, respectively). The first push (FP) difference consisted of recording spectrum 1 after cooling from dark state (200 scans) and subtracting from spectrum recorded after the sample was illuminated with a 505 nm LED in the case of *Ca*ChR1 and a 455 nm LED in the case of *Cr*ChR2, as described in the Materials and Methods. Y-axis markers are approximately 2 mOD for *Ca*ChR1 and 0.4 mOD for *Cr*ChR2.

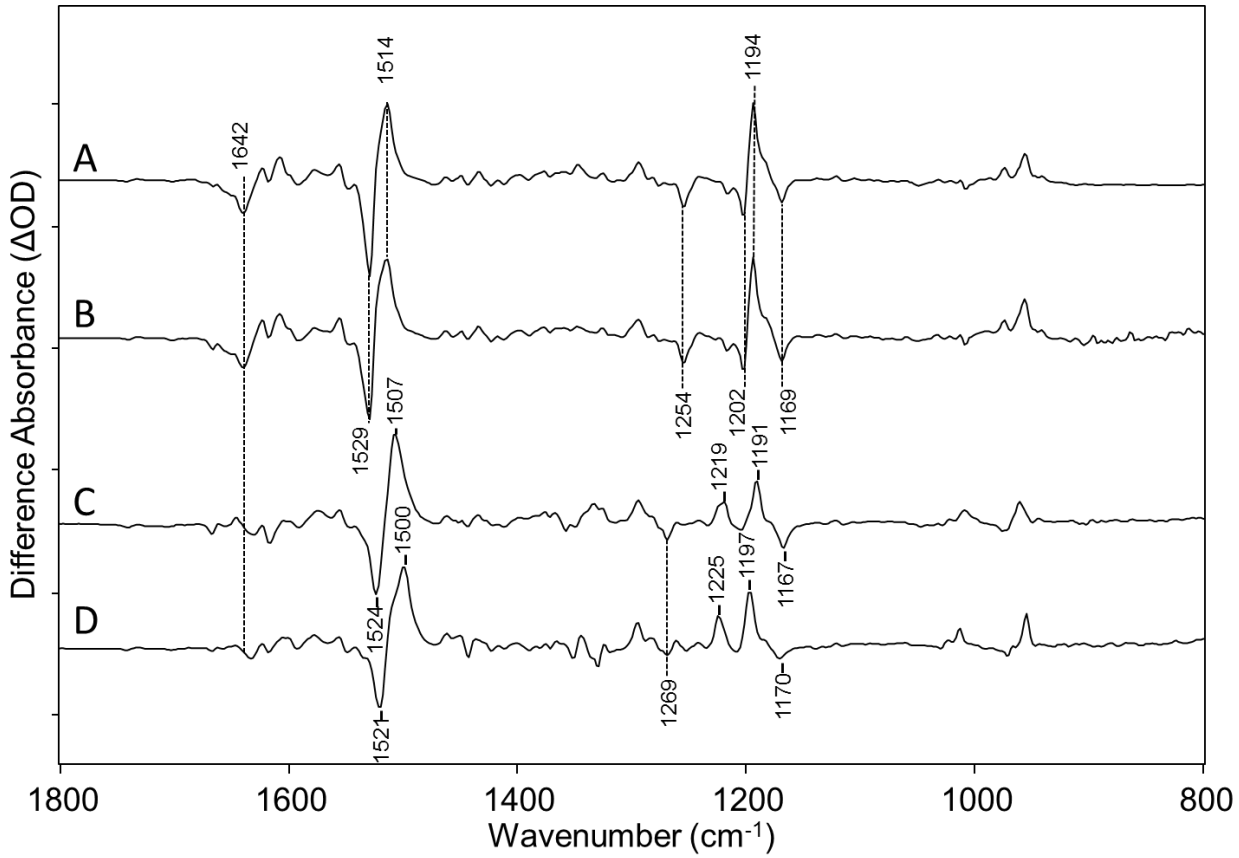

Figure S3: Comparison over the 800-1800 cm^{-1} region of light-adapted BR for : (A) native purple membrane containing the normal all-*trans* A1 retinal, (B) BR regenerated with A1 retinal after bleaching (C) regenerated with [15-^{13}C,15-^{2}H] retinal after bleaching and (D) regenerated with [14,15-$^{2}H_2$] retinal after bleaching. Y-axis markers are approximately 3 mOD for all spectra. See Materials and Methods for additional details.

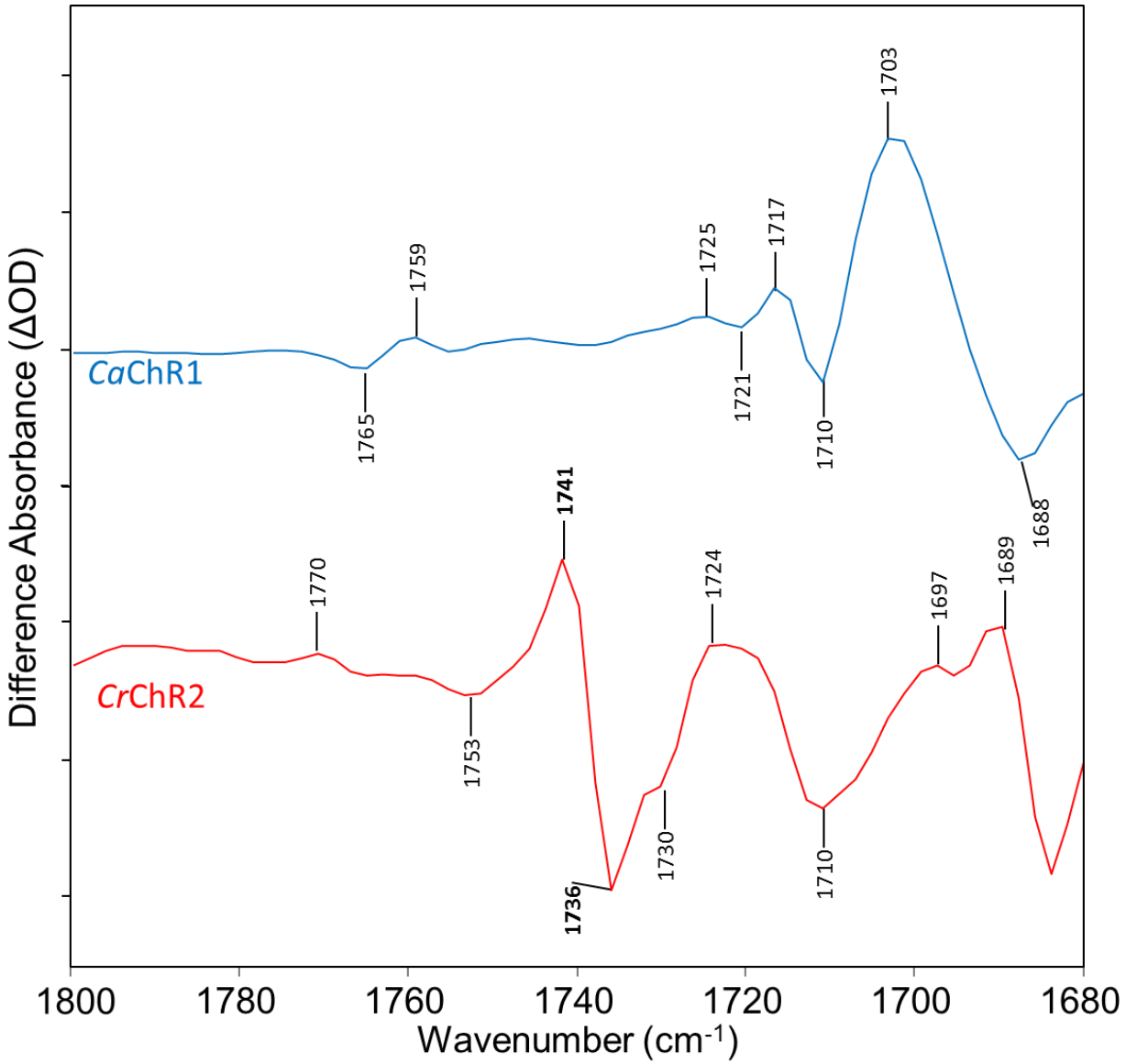

Figure S4: Comparison of *Ca*ChR1 (top, in blue) and *Cr*ChR2 (bottom, in red), over the 1680-1800 cm^{-1} region at 80 K. Y-axis markers are approximately 300 mOD for *Ca*ChR1 and 70 mOD for *Cr*ChR2. For additional acquisition and illumination parameters see the Materials and Methods section.

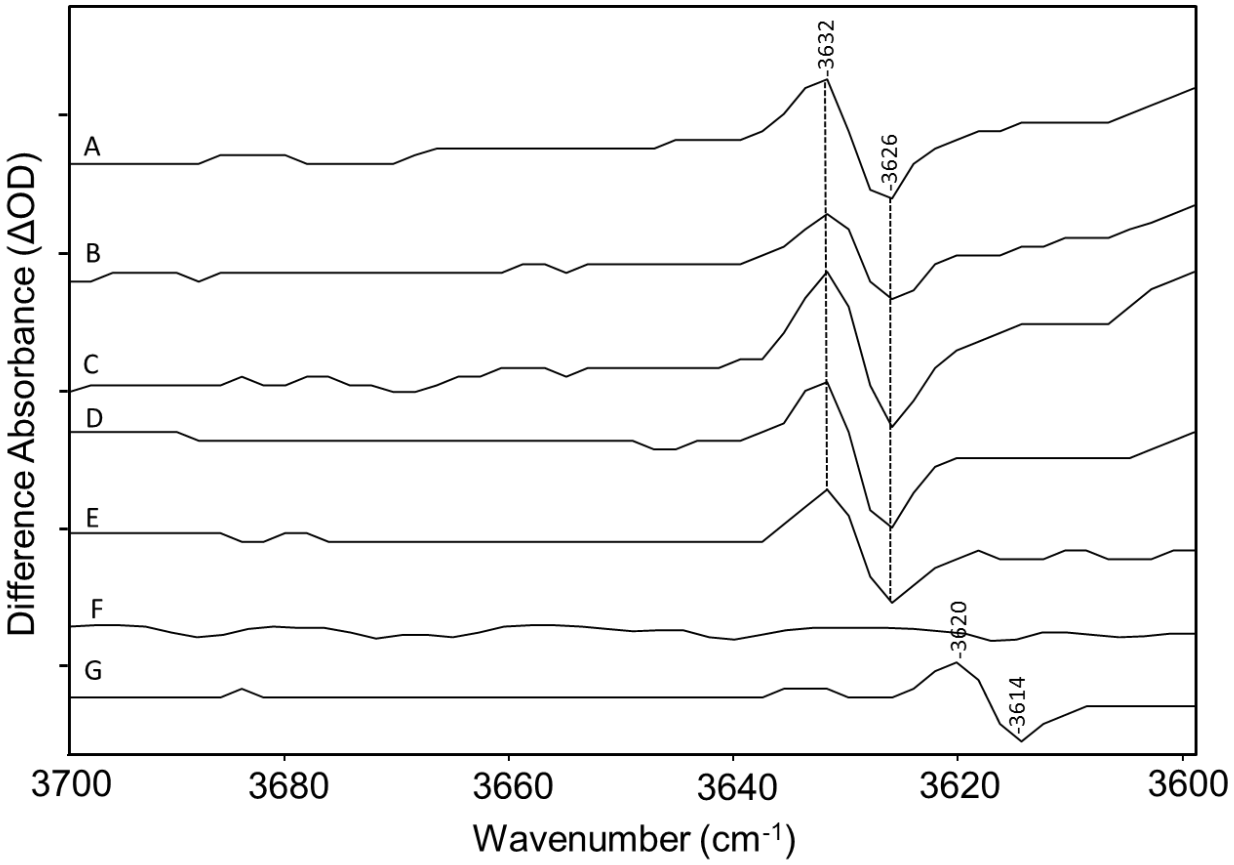

Figure S5: Spectra from Figure 7 of the paper over the 3600-3700 cm^{-1} region. (A) *Ca*ChR1 in H_2O, (B) regenerated with A1 retinal, (C) regenerated with A2 retinal, (D) regenerated with [15-^{13}C,15-^{2}H] retinal, (E) regenerated with [14,15-$^{2}H_2$] retinal, (F) *Ca*ChR1in D_2O, and (G) *Ca*ChR1 in $H_2{}^{18}O$. Y-axis markers are approximately 0.15 mOD for all spectra. For detailed bleaching and regeneration procedures as well as spectral acquisition parameters, see Materials and Methods.

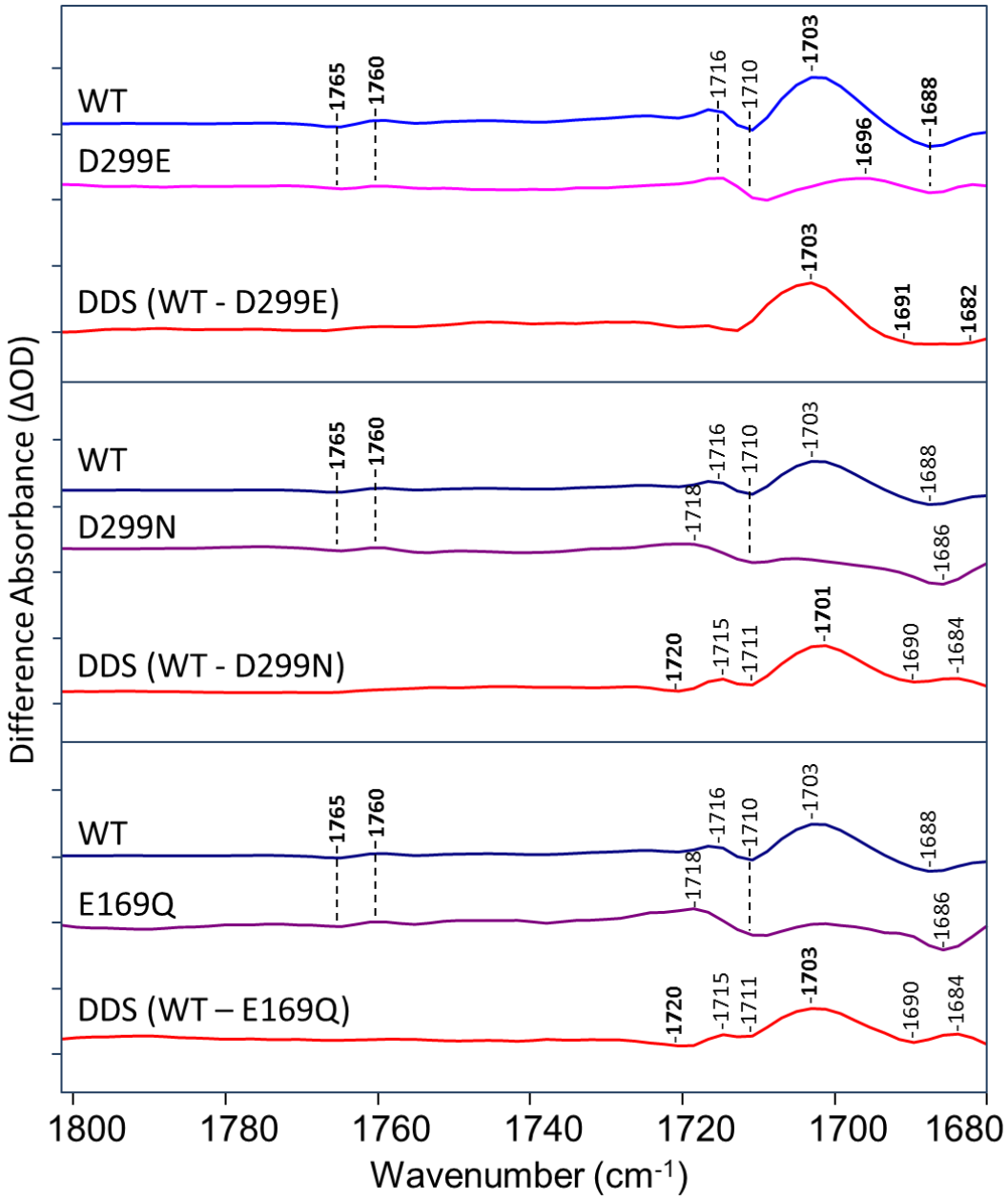

Figure S6. Difference FTIR and double difference FTIR of *Ca*ChR1 and its D299E, D299N, and E169Q mutants over the region from 1680-1800 cm^{-1}. Y-axis tick-marks are approximately 0.6, 0.6, 0.5, 0.1 mOD for WT, D299E, D299N, and E169Q, respectively.

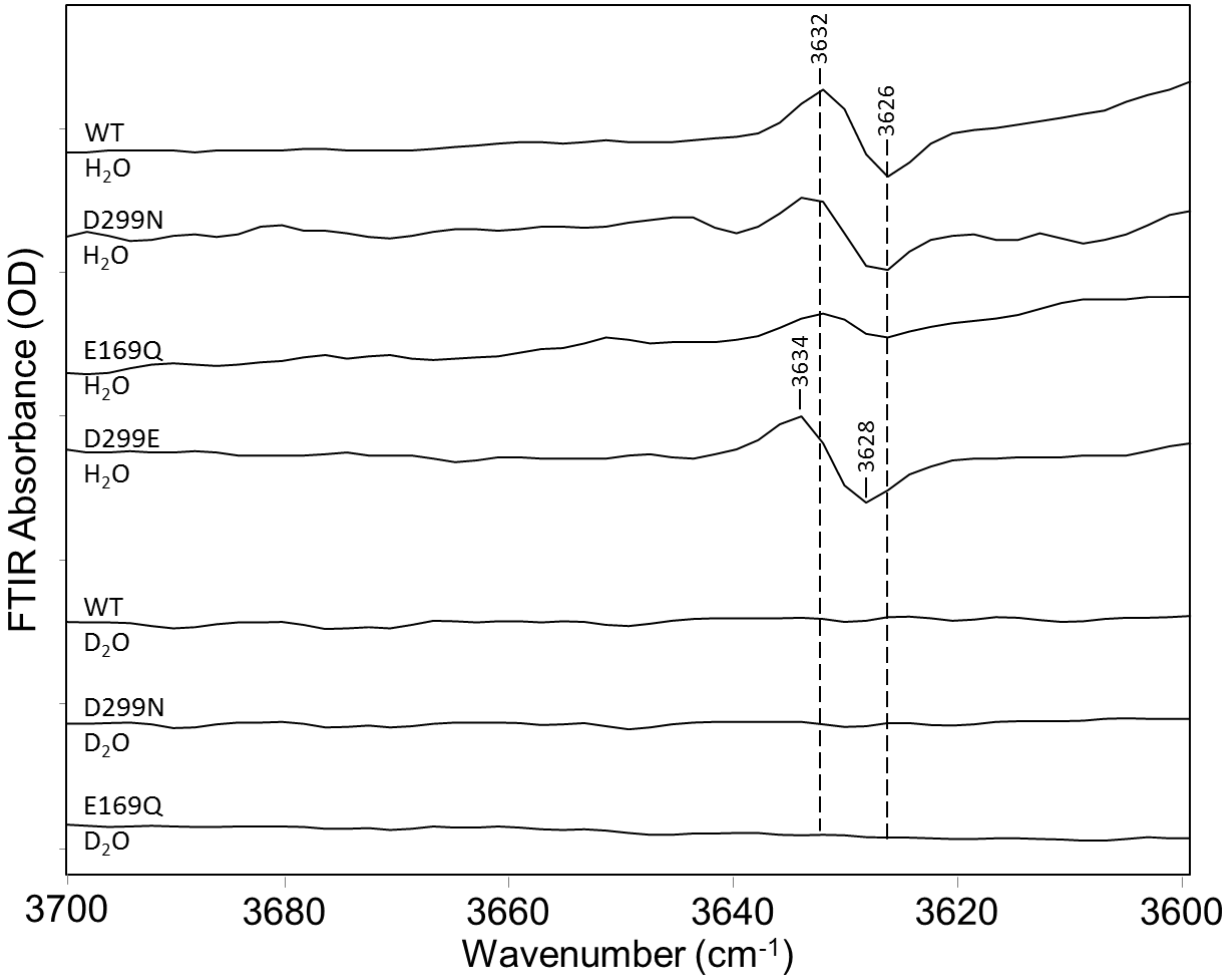

Figure S7: Comparison of *Ca*ChR1 WT and mutants over the 3600-3700 cm^{-1} region. The top four spectra were recorded in H_2O and the bottom three in D_2O. Y-axis markers are approximately 0.2 mOD for all spectra. For detailed H-D exchange and site-directed mutagenesis procedures as well as spectral acquisition parameters, see Materials and Methods.

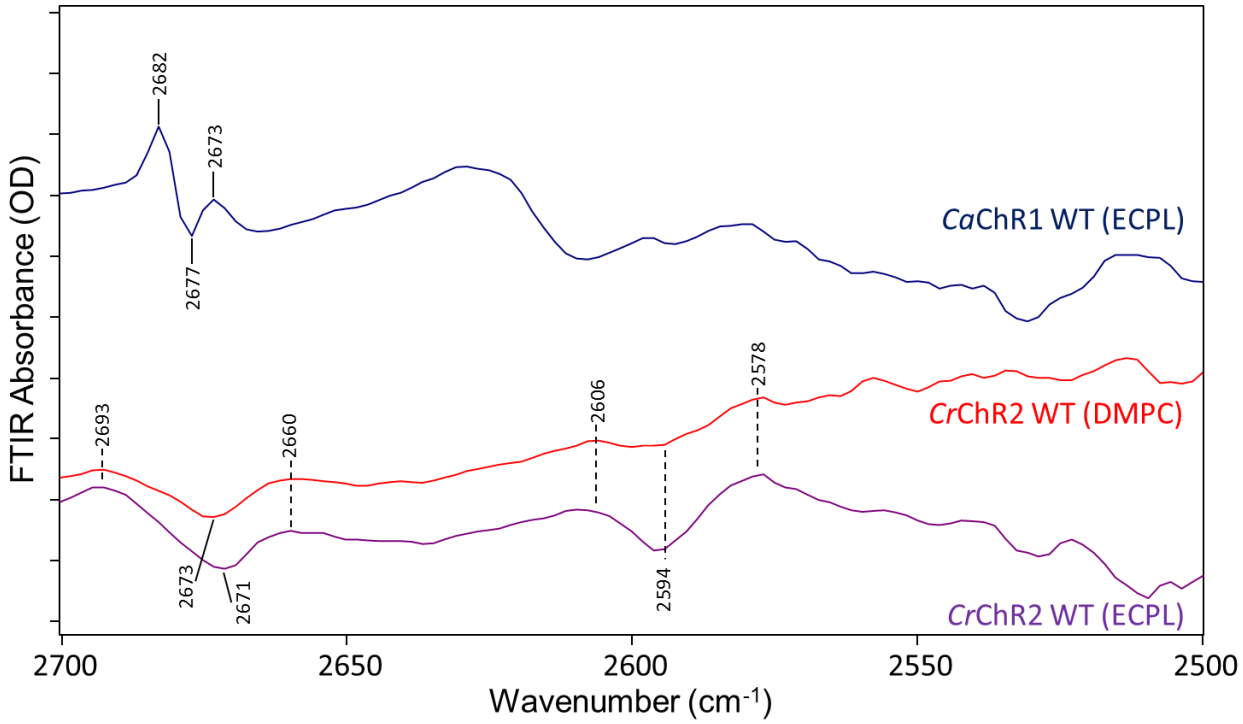

Figure S8: Comparison of *Ca*ChR1 in D_2O, *Cr*ChR2 in D_2O reconstituted in both DMPC and ECPL over the region from 2500-2700 cm^{-1} at 80 K. Y-axis markers represent approximately 0.05 mOD for all spectra.